

## A dominant vibration mode-based scalar ground motion intensity measure for single-layer reticulated domes

Jie Zhong<sup>1,2a</sup>, Xudong Zhi<sup>\*1,2</sup> and Feng Fan<sup>1,2b</sup>

<sup>1</sup>Key Laboratory of Structures Dynamic Behavior and Control of the Ministry of Education, Harbin Institute of Technology, Harbin 150090, China

<sup>2</sup>School of Civil Engineering, Harbin Institute of Technology, Harbin 150090, China

(Received April 23, 2015, Revised June 21, 2016, Accepted July 12, 2016)

**Abstract.** A suitable ground motion intensity measure ( $IM$ ) plays a crucial role in the seismic performance assessment of a structure. In this paper, we introduce a scalar  $IM$  for use in evaluating the seismic response of single-layer reticulated domes. This  $IM$  is defined as the weighted geometric mean of the spectral acceleration ordinates at the periods of the dominant vibration modes of the structure considered, and the modal strain energy ratio of each dominant vibration mode is the corresponding weight. Its applicability and superiority to 11 other existing  $IM$ s are firstly investigated in terms of correlation with the nonlinear seismic response, efficiency and sufficiency using the results of incremental dynamic analyses which are performed for a typical single-layer reticulated dome. The hazard computability of this newly proposed  $IM$  is also briefly discussed and illustrated. A conclusion is drawn that this dominant vibration mode-based scalar  $IM$  has the characteristics of strong correlation, high efficiency, good sufficiency as well as hazard computability, and thereby is appropriate for use in the prediction of seismic response of single-layer reticulated domes.

**Keywords:** ground motion intensity measure; nonlinear seismic response; single-layer reticulated domes; incremental dynamic analysis; modal strain energy ratio

### 1. Introduction

In performance-based earthquake engineering (PBEE), a ground motion intensity measure ( $IM$ ) plays an indispensable role in evaluating the seismic performance of a structure, where it should usually capture the salient attributes and quantify the strength of an earthquake ground motion. Traditionally, owing to the explicitness and simplicity, peak ground acceleration and, alternatively, peak ground velocity, denoted as PGA and PGV, respectively, have been commonly used in building codes and engineering practice. Meanwhile, spectral acceleration at the fundamental period of a given structure with a damping ratio of  $\zeta$ , denoted as  $S_a(T_1, \zeta)$  or  $S_a(T_1)$  for brevity, has also been widely adopted in the United States, such as the ATC-63 report (ATC 2009). Most

---

\*Corresponding author, Professor, E-mail: zhixudong@hit.edu.cn

<sup>a</sup>Ph.D., E-mail: zhjiehit@163.com

<sup>b</sup>Ph.D., E-mail: fanfhit@hit.edu.cn

recently, many studies have been carried out for the purpose of identifying or developing an optimal ground motion  $IM$  for different categories of conventional structures, such as bridges, reinforced concrete frame structures, or steel moment-resisting frame structures. These research findings suggested that the appropriateness and applicability of each  $IM$  differ among structures. Padgett *et al.* (2008) indicated that PGA is an optimal  $IM$  for a portfolio of bridges when the computability in seismic hazard analysis is considered. Shome (1999) found that, for short and moderate-period structures,  $S_a(T_1)$  is more efficient (i.e., the variability of seismic response for an  $IM$  level is lower) and more closely related to the seismic response. Kostinakis and Athanapoulou (2015) also indicated that  $S_a(T_1)$  is a relatively good  $IM$  for medium rise reinforced concrete buildings that possess small structural eccentricity. Luco and his coworkers presented some advanced  $IM$ s in their studies (e.g., Luco *et al.* 2005, Luco and Cornell 2007), like  $\{S_a(T_1), S_a(T_2)/S_a(T_1), S_a^D(T_1)/S_a(T_1)\}$ ,  $IM_{1E\&2E}$  or  $IM_{11\&2E}$ , which include a higher-mode spectral acceleration or displacement, and were demonstrated to be relatively more efficient and sufficient for tall, long-period buildings whose higher modes are also as important to the structural response as the fundamental mode. Cordova *et al.* (2000) developed a two-parameter  $IM$  based on  $S_a(T_1)$  and  $S_a(T_f)$ , i.e., the spectral acceleration at the lengthened period  $T_f$  due to structural softening. This  $IM$  is capable of reflecting the spectral shape and the period shift effect under stiffness degradation. In order to account for wider range of the acceleration response spectrum that may be important for either the high-mode effects or the nonlinear behavior of a structure, Bianchini and Diotallevi (2009) defined  $S_{a, avg}(T_1, \dots, T_n)$ , or briefly  $S_{a, avg}$ , as the geometric mean of spectral acceleration ordinates over a certain range of periods, which was demonstrated to be an optimal scalar  $IM$  to predict inelastic structural response of buildings subjected to recorded ground motions, and Bojórquez and Iervolino (2011) devised a vector-valued  $IM$ ,  $\langle S_a, N_p \rangle$ , and a scalar  $IM$ ,  $I_{N_p}$ , using a parameter proxy for the spectral shape, i.e.,  $N_p$ , to incorporate more periods of interest.

Obviously, almost all the aforementioned efforts were dedicated to conventional building structures, and as of today, very little work has been done to investigate what  $IM$  is applicable to long-span spatial lattice structures, typically represented by reticulated domes and space truss structures. In the last three decades, these structures have been widely used in gymnasiums, conference and exhibition centers, airport terminal buildings, etc. The engineering practice and research studies showed that the structures of this category exhibit especially closely spaced frequencies as well as complex vibration modes and the calculation of their seismic response using mode superposition methods (CQC or SRSS) usually requires a few tens of higher modes to be involved. It was also showed that the number of dominant modes and the magnitude of contribution of each dominant mode to the total response of a structure vary from motion to motion, due to the fact that the frequency content of each ground motion differs from that of one another. As a result, an optimal  $IM$  for these structures should consider as many of these factors as possible. The study presented by Fan *et al.* (2012) was an effort to do this. They proposed a new scalar  $IM$  based on a reticulated dome, i.e., spectral acceleration at the peak response frequency ( $f_p$ , the frequency at which the structure attains its peak response in a harmonic response analysis), denoted as  $S_a(f_p)$ , and suggested that this  $IM$  is more strongly correlated with the seismic response than  $S_a(T_1)$  when the dome is subjected to unidirectional vertical seismic excitation only, since the seismic response in this case is basically dominated by the individual higher mode at the peak response frequency. However, it still fails to include more information about both the modal properties of the dome and the frequency content of a ground motion, and hence it was demonstrated to be not as successful as in the preceding case when the dome was subjected to

unidirectional horizontal or tri-directional seismic excitation, in which cases, the magnitude of contribution of any dominant mode to the total seismic response is not overwhelming. To overcome this drawback, therefore, the present study seeks to present a new scalar *IM* on the basis of reticulated domes subjected to different cases of seismic excitation. This *IM* must have the capability to take account of more characteristics of the dominant vibration modes, capture more frequency content information of a ground motion, as well as balance the weight of each individual dominant mode according to its magnitude of contribution to total seismic response.

## 2. Structural modeling and modal analysis

### 2.1 Structural modeling

Single-layer reticulated domes constitute a special category of structures in which individual straight members are connected at joints in a manner that permits no rotation. The geometry and layout of a Kiewitt-8 single-layer reticulated dome are illustrated in Fig. 1. The dome considered in this paper has a span of  $L=60$  m and a height-to-span ratio of  $f/L=1/5$ , which is within the range of  $1/7$  to  $1/3$  in accordance with the recommendations for practical construction in the technical specification for space frame structures (JGJ 7-2010). The reticulated dome considered consists of 289 joints and 800 individual structural members, which are usually divided into three groups: radial, ring, and oblique members. The material adopted for the initially undamaged state is elastoplastic steel, with a yield stress of  $\sigma_y=235$  N/mm<sup>2</sup> and a Young's modulus of  $E=2.06\times 10^5$  N/mm<sup>2</sup>, and the continuous deterioration of material properties due to damage accumulation is taken into consideration (refer to Nie *et al.* (2012) for more details). The damping ratio  $\zeta$  in each mode of the structure is set to 0.02 according to JGJ 7-2010. The Rayleigh damping is employed for nonlinear time history analyses, and the stiffness and mass proportionality factors are 0.274 and  $1.461\times 10^{-3}$ , respectively, which were evaluated using the first two vibration modes, due to the fact that these modes give the two largest contributions to the total seismic response. All the boundary nodes of the reticulated dome are hinged supports. The roof weight is 180 kg/m<sup>2</sup>, which includes a dead load of 160 kg/m<sup>2</sup> and one-half a live load of 40 kg/m<sup>2</sup>. According to JGJ 7-2010, the consistent imperfection mode method was adopted to compute the initial geometrical imperfection with an imperfection amplitude of  $L/1500$ . Steel pipe sizes were determined using common static design procedures, including the assurance of structural stability under static loads by employing a safety factor of 2.0. For the details of the steel pipe sizes, see Table 1.

The finite element model of the reticulated dome in this paper was established using the finite element software ABAQUS 6.12. Each individual structural member is represented by element type B31 available in ABAQUS/Standard. B31 is a type of three-dimensional, 2-node linear beam element, with the capabilities of tension-compression, bending, and torsion. Each node has six degrees of freedom and each cross-section has 8 integration points, as shown in Fig. 2.

Table 1 Parameters of the Kiewitt-8 single-layer reticulated dome

$L$ (m)	$f/L$	Roof Weight (kg/m <sup>2</sup> )	Member size (mm)			Fundamental frequency (Hz)	$f_p$ (Hz)	
			Radial	Ring	Oblique		X	Z
60	1/5	180	$\phi 140\times 5$	$\phi 133\times 4$	$\phi 133\times 4$	2.18	2.18	4.74

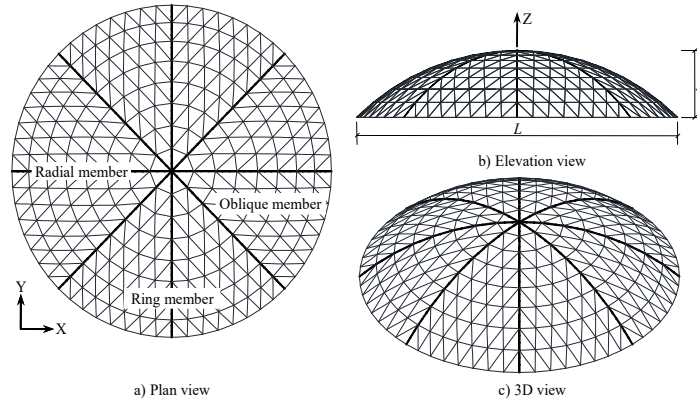


Fig. 1 Geometry and layout of the Kiewitt-8 single-layer reticulated dome

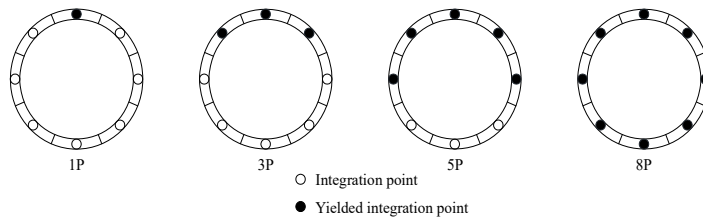


Fig. 2 Definition of different levels of plastic deformation for the cross-section of the ABAQUS/Standard element type B31

2.2 Modal analysis

Modal analysis of the reticulated dome described above was carried out to investigate its dynamic properties. Fig. 3 shows the distribution of natural vibration frequencies for the first 400 vibration modes ranging from 2.18 to 26.73 Hz, and Fig. 4 presents several representative modes of vibration of this reticulated dome.

As seen in Figs. 3-4, the natural vibration frequencies of the reticulated dome are very closely

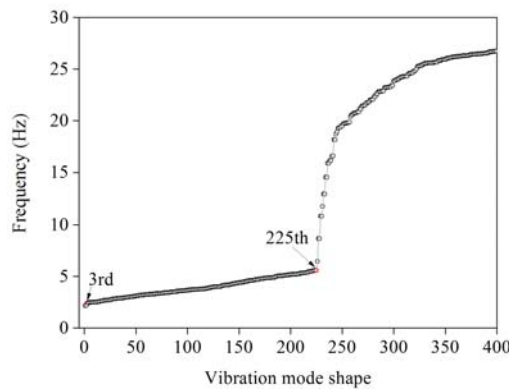


Fig. 3 Distribution of the natural vibration frequencies of the reticulated dome

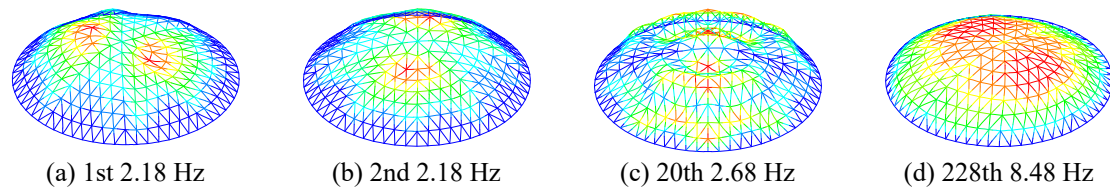


Fig. 4 Several representative vibration mode shapes of the reticulated dome

spaced, and the vibration modes are quite complex, which can be categorized into three types: the first type is horizontal vibration (Figs. 4(a)-(b)), represented by the 1st and 2nd modes; the second is coupled horizontal and vertical vibration (Fig. 4(c)), whose frequencies range from the 3rd to the 225th; and the last one is local or in-plane vibration (Fig. 4(d)), the frequencies of which are much higher than that of the former two types.

### 3. Historical ground motion records and 11 common *I*Ms

#### 3.1 Historical ground motion records

A suite of 20 recorded ground motions were selected from the PEER-NGA strong motion database (<http://ngawest2.berkeley.edu/>), which contains a total of 173 earthquakes from California, Japan, Taiwan, and other seismically active regions, with a sum of 3,551 ground motion records. The recordings employed in the present study were chosen from 11 earthquakes with moment magnitudes ( $M_w$ ) greater than 6.0. The closest site-to-fault-rupture distances ( $R_{clst}$ ) are between 10 and 30 km, and the near-fault ground motions with an average Campbell and Joyner-Boore fault distance less than 10 km were excluded. The fault rupture mechanisms involve strike-slip, reverse, and reverse-oblique. According to the definition of the NEHRP (BSSC 1997) provisions based on the average shear-wave velocity in the upper 30 m ( $V_{s,30}$ ), the site classes are Class C (very dense soil and soft rock with  $360 \text{ m/s} < V_{s,30} \leq 760 \text{ m/s}$ ) and Class D (stiff soil with  $180 \text{ m/s} < V_{s,30} \leq 360 \text{ m/s}$ ), which approximately correspond to Site Class II in Chinese codes (GB50011-2010, JGJ7-2010). Apart from these criteria, the corner frequency of the high-pass filter is less than 0.25 Hz, and each ground motion should consist of two horizontal components and one vertical component, which dictates that the records without vertical components must not be included. Table 2 lists the details of the 20 selected ground motion recordings.

Table 2 Characteristics of the 20 selected ground motions

ID No.	Earthquake Name	Year	Station Name	$M_w$	$R_{clst}$ (km)	Site Class
1	Imperial Valley-06	1979	Delta	6.53	22.03	D
2	Superstition Hills-02	1987	El Centro Imp. Co. Cent	6.54	18.20	D
3	Superstition Hills-02	1987	Westmorland Fire Sta	6.54	13.03	D
4	Loma Prieta	1989	Capitola	6.93	15.23	D
5	Northridge-01	1994	Beverly Hills-14145 Mulhol	6.69	17.15	D
6	Loma Prieta	1989	Gilroy Array #3	6.93	12.82	D

Table 2 Continued

ID No.	Earthquake Name	Year	Station Name	$M_w$	$R_{clst}$ (km)	Site Class
7	Kobe, Japan	1995	Shin-Osaka	6.90	19.15	D
8	Friuli, Italy-01	1976	Tolmezzo	6.50	15.82	C
9	Northridge-01	1994	Canyon Country-W Lost Cany	6.69	12.44	D
10	Imperial Valley-06	1979	El Centro Array #11	6.53	12.45	D
11	San Fernando	1971	LA-Hollywood Stor FF	6.61	22.77	D
12	Cape Mendocino	1992	Rio Dell Overpass-FF	7.01	14.33	D
13	Landers	1992	Yermo Fire Station	7.28	23.62	D
14	Kocaeli, Turkey	1999	Arcelik	7.51	13.49	C
15	Manjil, Iran	1990	Abbar	7.37	12.56	C
16	Chi-Chi, Taiwan	1999	TCU045	7.62	26.00	C
17	Landers	1992	Coolwater	7.28	19.74	D
18	Duzce, Turkey	1999	Bolu	7.14	12.04	D
19	Hector Mine	1999	Hector	7.13	11.66	C
20	Kocaeli, Turkey	1999	Duzce	7.51	15.37	D

Table 3 Descriptions of 11 common *IMs*

<i>IM</i>	Description	Units
<i>PGA</i>	Peak ground acceleration, $PGA = \max  \ddot{u}_g(t) $	g
<i>PGV</i>	Peak ground velocity, $PGV = \max  \dot{u}(t) $	cm/s
<i>PGD</i>	Peak ground displacement, $PGD = \max  u(t) $	cm
<i>AI</i>	Arias intensity, $AI = \frac{\pi}{2g} \int_0^{t_f} [\ddot{u}_g(t)]^2 dt$	cm/s
<i>CAV</i>	Cumulative absolute velocity, $CAV = \int_0^{t_f}  \ddot{u}_g(t)  dt$	cm/s
<i>ASI</i>	Acceleration spectrum intensity, $ASI = \int_0^{0.5} S_a(\xi = 0.02, T) dT$	g
<i>VSI</i>	Velocity spectrum intensity, $VSI = \int_0^{2.5} S_v(\xi = 0.02, T) dT$	cm/s
$S_a(T_1)$	Spectral acceleration at the fundamental period $T_1$ .	g
$S_a(f_p)$	Spectral acceleration at the peak response frequency $f_p$ .	g
$S_{a, avg}$	Geometric mean of the spectral acceleration at the $n$ periods of interest, $S_{a, avg}(T_1, \dots, T_n) = \left( \prod_1^n S_a(T_i) \right)^{1/n}$	g
$I_{Np}$	A scalar <i>IM</i> based on the first mode spectral acceleration and a parameter proxy for the spectral shape, i.e., $N_p$ , $I_{Np} = S_a(T_1) N_p^\alpha$	g

### 3.2 Descriptions of 11 Common *IMs*

As mentioned above, an *IM* usually captures the salient attributes of a ground motion, and

characterizes its relationship in association with a hazard level as well as the magnitude of the structural response. In the present study, 11 common *IMs* that have been the subject of previous studies and are frequently used in engineering practice were selected to quantify each of the aforementioned 20 ground motions as well as to scale them to desired levels when performing nonlinear dynamic time history analysis, and to carry out comparisons with the new *IM* to be introduced in Section 4 for the purpose of examining whether the newly proposed *IM* is more appropriate for single-layer reticulated domes. Detailed descriptions of these *IMs* are summarized in Table 3. These *IMs* reflect different characteristics of a ground motion. More specifically, other than PGA, PGV,  $S_a(T_1)$ ,  $S_a(f_p)$ ,  $S_{a,avg}$  and  $I_{Np}$ , which have already been defined, PGD represents the peak displacement time history, AI and CAV represent a type of *IM* based on an integration over time of the acceleration time history, and the remaining *IMs*, i.e., ASI and VSI, are obtained respectively from the integration of the spectral acceleration and velocity over a range of spectral periods. It is worth mentioning that for tri-directional seismic excitation case, all the above 11 *IMs* were taken as the SRSS combination of the corresponding values of the two horizontal and one vertical component of the ground motion.

#### 4. A dominant vibration mode-based scalar ground motion *IM*

A scalar *IM* is proposed in this paper, taking into account more frequency content information of an earthquake ground motion and more salient vibrational characteristics of a structure. More specifically, the newly proposed *IM*, denoted as  $S_{a,dom}(T_1^d, T_2^d, \dots, T_i^d, \dots, T_N^d, \xi)$ , or  $S_{a,dom}$  for brevity, is defined as the weighted geometric mean of the spectral acceleration ordinates at the periods set  $T_1^d, \dots, T_N^d$  associated with  $N$  dominant vibration modes, and the modal strain energy ratio  $r_i$  of each dominant mode is the corresponding weight. Mathematically, this new *IM* is given as

$$S_{a,dom}(T_1^d, T_2^d, \dots, T_i^d, \dots, T_N^d, \xi) = \prod_{i=1}^N (S_a(T_i^d, \xi))^{r_i} \quad (1)$$

in which  $T_i^d$  is identified and extracted by utilizing  $r_i$ , as detailed below.

##### 4.1 Theory for the modal strain energy ratio

For a structure under three-dimensional seismic excitation, the dynamic force equilibrium as a function of time can be expressed by the differential equation

$$\mathbf{M}\ddot{\mathbf{u}}(t) + \mathbf{C}\dot{\mathbf{u}}(t) + \mathbf{K}\mathbf{u}(t) = -\mathbf{M}_x\ddot{u}(t)_{xg} - \mathbf{M}_y\ddot{u}(t)_{yg} - \mathbf{M}_z\ddot{u}(t)_{zg} \quad (2)$$

in which  $\mathbf{M}$  is the mass matrix,  $\mathbf{C}$  is the viscous damping matrix, and  $\mathbf{K}$  is the static stiffness matrix. The time-dependent vectors  $\ddot{\mathbf{u}}(t)$ ,  $\dot{\mathbf{u}}(t)$ , and  $\mathbf{u}(t)$  are the node accelerations, velocities, and displacements relative to the three corresponding components of the free-field ground, respectively.  $\mathbf{M}_j$  is equal to  $\mathbf{M}\mathbf{I}_j$ , where  $\mathbf{I}_j$  is a vector with ones in the “ $j$ ” directional degrees of freedom and zero in all other positions, and  $\ddot{u}(t)_{jg}$  are the three components of the free-field ground motion acceleration.

Using the mode superposition method, the total relative displacement for the  $i$ -th mode is

$$\mathbf{u}_i(t) = \gamma_{ix}\phi_{ix}D_{ix}(t) + \gamma_{iy}\phi_{iy}D_{iy}(t) + \gamma_{iz}\phi_{iz}D_{iz}(t) \quad (3)$$

where  $\phi_i$  is the  $i$ -th natural mode of vibration, and  $\gamma_{ij}$  is the  $i$ -th modal participation factor, as defined by Chopra (2001), and  $D_{ij}(t)$  is the displacement for the  $i$ -th mode of a single-degree of freedom due to the ground motion  $\ddot{u}(t)_{jg}$  for  $j$  equal to  $x$ ,  $y$ , or  $z$ . Hence, the modal strain energy for the  $i$ -th mode expressed in the form of Eq. (4) can be rewritten as Eq. (5)

$$E_i(t) = \frac{1}{2} \mathbf{u}_i(t)^T [\mathbf{K}] \mathbf{u}_i(t) \quad (4)$$

$$E_i(t) = \frac{1}{2} [\gamma_{ix} D_{ix}(t) + \gamma_{iy} D_{iy}(t) + \gamma_{iz} D_{iz}(t)]^2 \phi_i^T [\mathbf{K}] \phi_i \quad (5)$$

Note that  $\phi_i^T [\mathbf{K}] \phi_i$  can be replaced by  $M_i \omega_i^2$  in which  $M_i$  is the generalized mass of the  $i$ -th normal mode and  $\omega_i$  is the natural circular frequency associated with the  $i$ -th mode. Therefore, the modal strain energy of Eq. (5) can also be expressed as follows

$$E_i(t) = \frac{1}{2} M \left[ M_{rix}^* V_{ix}^2(t) + M_{riy}^* V_{iy}^2(t) + M_{riz}^* V_{iz}^2(t) \right] \\ + M_i [\gamma_{ix} \gamma_{iy} V_{ix}(t) V_{iy}(t) + \gamma_{iy} \gamma_{iz} V_{iy}(t) V_{iz}(t) + \gamma_{ix} \gamma_{iz} V_{ix}(t) V_{iz}(t)] \quad (6)$$

Here,  $M$  is the total mass of the structure,  $M_{ij}^*$  is the effective mass for the  $i$ -th mode in the direction  $j$ , and  $M_{rij}^* = M_{ij}^*/M$  is the ratio of effective mass to total mass.  $V_{ij}(t) = D_{ij}(t)\omega_i$ , is the relative velocity for the  $i$ -th mode. One may note that the last term in Eq. (6) is equal to zero. Therefore, the modal strain energy for the  $i$ -th mode can be written as

$$E_i(t) = \frac{1}{2} M \left[ M_{rix}^* V_{ix}^2(t) + M_{riy}^* V_{iy}^2(t) + M_{riz}^* V_{iz}^2(t) \right] \quad (7)$$

Because only a single term on the right-hand side of Eq. (7) dominates the modal strain energy for a given mode, the modal strain energy can be obtained by introducing the spectral pseudo-velocity  $S_{vij}$  as

$$E_i = \frac{1}{2} M \left[ M_{rix}^* S_{vix}^2 + M_{riy}^* S_{viy}^2 + M_{riz}^* S_{viz}^2 \right] \quad (8)$$

Then, the total modal strain energy can be computed by

$$E = \sum_{i=1}^N E_i = \frac{1}{2} M \sum_{i=1}^N \left[ M_{rix}^* S_{vix}^2 + M_{riy}^* S_{viy}^2 + M_{riz}^* S_{viz}^2 \right] \quad (9)$$

Here, the modal strain energy ratio for the  $i$ -th mode can be defined as

$$r_i = \frac{E_i}{\sum_{j=1}^N E_j} = \frac{M_{rix}^* S_{vix}^2 + M_{riy}^* S_{viy}^2 + M_{riz}^* S_{viz}^2}{\sum_{j=1}^N \left[ M_{rjx}^* S_{vjx}^2 + M_{rjy}^* S_{vjy}^2 + M_{rjz}^* S_{vjz}^2 \right]} \quad (10)$$

For the case where the structure is subjected only to unidirectional seismic excitation, in the X-direction for example, the modal strain energy and the corresponding ratio can be given as

follows

$$E_{ix} = \frac{1}{2} M M_{rix}^* S_{vix}^2 \tag{11}$$

$$r_{ix} = \frac{E_i}{\sum_{j=1}^N E_j} = \frac{M_{rix}^* S_{vix}^2}{\sum_{j=1}^N M_{rjx}^* S_{vjx}^2} \tag{12}$$

One should note that the calculation of  $r_i$  involves not only the effective mass ratios of each mode but also the pseudo-velocity response spectra of an earthquake ground motion. Obviously, this makes the value of  $r_i$  vary from motion to motion, rather than retain a constant value, which implies that it is more capable of reflecting the magnitude of contribution of each individual vibration mode to the total seismic response. In the literature (e.g., Kato *et al.* 2007, Yang *et al.* 2010), it has been utilized to identify the modes which are significantly contributory to the total seismic response of long-span latticed spatial structures. Likewise, in this paper, it is used to identify and extract the dominant modes of the considered single-layer reticulated dome under different ground motions, and then compute the newly proposed  $S_{a, dom}$  for each ground motion.

#### 4.2 Illustration of the calculation of $S_{a, dom}$

To offer a better understanding of how the dominant vibration modes of a single-layer reticulated dome are identified and extracted via the modal strain energy ratio and how the newly proposed  $S_{a, dom}$  is calculated, the single-layer reticulated dome described in Section 2.1 is here

Table 4 Calculation of  $S_{a, dom}$  of a unidirectional horizontal ground motion

Mode #	Frequency (Hz)	$M_{rix}^*$	$S_{vix}$ (m/s)	$S_{aix}^*$ (m/s <sup>2</sup> )	$E_{ix}$ (J)	$r_{ix}$
1	2.179	0.056	0.094	1.292	155.491	0.072
2	2.179	0.140	0.094	1.292	389.024	0.180
7	2.485	0.066	0.137	2.162	385.533	0.179
8	2.485	0.012	0.137	2.162	67.737	0.031
19	2.677	0.027	0.167	2.779	231.813	0.108
20	2.677	0.037	0.167	2.779	320.455	0.149
28	2.809	0.022	0.153	2.714	157.410	0.073
33	2.870	0.013	0.145	2.594	84.601	0.039
40	2.959	0.012	0.132	2.457	66.991	0.031
52	3.104	0.012	0.114	2.257	49.974	0.023
228	8.642	0.335	0.047	2.645	235.738	0.109

\*  $S_{aix}$  : Pseudo-spectral acceleration associated with mode  $i$ ; and

$$S_{a, dom} = \prod_{i=1}^N (S_{aix}(T_i^d, \xi))^{r_{ix}} = 2.121 \text{ m/s}^2$$

assumed to be subjected to unidirectional horizontal seismic excitation. The horizontal component with a larger PGA value of first ground motion listed in Table 2 is chosen as the input acceleration, and a step-by-step procedure for identifying and extracting the dominant vibration modes and computing  $S_{a, dom}$  is given as follows.

**Step 1:** Conduct a modal analysis of the reticulated dome, and extract parameters including frequencies, modal participation factors, and effective masses of the first 400 vibration modes and the total mass of the reticulated dome.

**Step 2:** Calculate pseudo-velocity and pseudo-acceleration response spectra of the selected ground motion and determine the corresponding values at or near the period of each of the first 400 modes.

**Step 3:** Compute the modal strain energy for each mode using Eq. (8), and the corresponding ratio using Eq. (12). Identify the dominant modes whose modal strain energy ratios are larger than a cutoff value, which is, here, assumed to be a small value of 0.02 for the sake of greater accuracy.

**Step 4:** Determine the pseudo-spectral acceleration value related to the period of each dominant mode. Calculate  $S_{a, dom}$  using Eq. (1) for unidirectional horizontal ground motion.

Table 4 lists the corresponding outcomes from the above four steps in the case of unidirectional horizontal ground motion excitation.

## 5. Structural response measures

For conventional structures, a variety of response measures have been proposed to quantify the damage state of a structure subjected to different levels of seismic excitation. For instance, numerous studies available in the literature (e.g., Luco *et al.* 2005, Jayaram *et al.* 2010) have indicated that peak (over time) interstory drift ratios (i.e., interstory drift divided by the height of the story, each denoted as  $IDR_i$  for story  $i$ ) are well correlated with both local demands and damage, and with the global stability of steel moment-resisting frames, reinforced concrete frames, and many other building types. However, previous studies have determined that these response measures are inappropriate for the seismic response and damage evaluation of complex, long-span spatial lattice structures, such as single-layer reticulated domes, and, as a result, the displacement of the vertex, or the maximum displacement over all the nodes of the dome has been adopted to quantify the damage of single-layer reticulated domes (e.g., Fan *et al.* 2012). While this is accurate and appropriate in the linear response case, when it comes to the case of nonlinear response, the displacement-based response measures are unable to capture other more key information, for example, the development of plastic strain. For the purpose of quantifying the seismic response and damage state of a dome more accurately, a more comprehensive response measure, denoted as the damage index  $DI$ , was proposed by Zhi *et al.* (2012), which is expressed as

$$DI = \alpha_i \times \sqrt{(f/L) \cdot (100 \times ((\frac{d_m - d_e}{L})^2 + (\frac{\varepsilon_a}{\varepsilon_u})^2) + r_1^2 + r_8^2)}, \quad (13)$$

where  $\alpha_i$  is a coefficient related to the structure type, which is 1.3 for the Kiewitt-8 single-layer reticulated dome (Zhi *et al.* 2012),  $d_m$  is the maximum displacement over all nodes,  $d_e$  is the maximum elastic displacement,  $\varepsilon_a$  is the average plastic strain over all members,  $\varepsilon_u$  is the ultimate strain of steel under axial tension, and  $r_1$  and  $r_8$  are ratios of members with different levels of plastic deformation on the cross-section (i.e., 1P and 8P, respectively, as illustrated in Fig. 2). The

value of  $DI$  reflects the damage level of a single-layer reticulated dome as a whole, where 0.0 indicates no damage and 1.0 or larger indicates collapse. Zhi *et al.* (2012) suggested that  $DI$  incorporates more key information of the seismic response, and is a more appropriate and accurate response measure when compared to the displacement-based response measures in the context of nonlinear response. Therefore, it is chosen as the structural response measure in the present study.

## 6. Characteristics of an optimal $IM$

In the literature (e.g., Cornell *et al.* 2002, Ellingwood *et al.* 2007, Nielson and DesRoches 2007), the structural response at each given  $IM$  level is typically assumed to be lognormally distributed so that the relationship between a structural response measure  $D$  and an  $IM$  can be expressed by a power law model as follows

$$D = a \cdot (IM)^b \cdot (\varepsilon | IM), \quad (14)$$

where  $a$  and  $b$  are regression coefficients and  $\varepsilon | IM$  is the error term. Using logarithmic transformation, the above exponential expression can be converted into Eq. (15) as follows

$$\ln(D) = \beta_0 + \beta_1 \ln(IM) + \ln(\varepsilon | IM), \quad (15)$$

where  $\beta_0$  and  $\beta_1$  are the linear regression coefficients. The regression coefficients can be obtained via simple linear regression of the natural logarithms of the resulting structural response data derived from incremental dynamic analyses (Vamvatsikos and Cornell 2002) on the corresponding values of different levels of a given  $IM$ .

The regression results are often utilized to investigate the appropriateness of a potential  $IM$  in terms of correlation with structural response measures, efficiency and sufficiency. The correlation can be examined using Pearson's correlation coefficient  $\rho$ , which is given as

$$\rho = \frac{\sum_1^N [\ln(IM_i) - m_{\ln(IM)}] \cdot [\ln(D_i) - m_{\ln(D)}]}{\sqrt{\sum_1^N [\ln(IM_i) - m_{\ln(IM)}]^2 \cdot \sum_1^N [\ln(D_i) - m_{\ln(D)}]^2}}, \quad (16)$$

where  $IM_i$  is the scaling level of a given  $IM$ ,  $D_i$  is the resulting structural response,  $m_{\ln(IM)}$  and  $m_{\ln(D)}$  are respectively the averages of  $\ln(IM)$  and  $\ln(D)$ , and  $N$  is the total number of the resulting data pairs. The  $IM$  metric referred to as efficiency can be evaluated by the standard deviation of the regression model, which is computed by

$$\beta_{\ln(D|IM)} = \sqrt{\frac{\sum_1^N (\ln(D_i) - m_{\ln(D|IM)})^2}{N - 2}}. \quad (17)$$

The value of  $\beta_{\ln(D|IM)}$  represents the amount of variation of the estimated structural response for a given  $IM$  value, and a more efficient  $IM$  with a lower  $\beta_{\ln(D|IM)}$  produces lower dispersion about the estimated median in the results of the incremental dynamic analyses, and, thereby, increases the accuracy of the empirical predictive model of seismic response and reduces the number of input ground motion records. The  $IM$  metric referred to as sufficiency is utilized as a viable measure to

identify the appropriateness of an *IM* for use in developing a probabilistic seismic demand model (PSDM) (Shome *et al.* 1998). A sufficient *IM* is conditionally independent from other parameters of a ground motion such as  $M_w$  or  $R_{clst}$ . The sufficiency of an *IM* can be examined via performing a linear regression of the residuals  $\ln(\varepsilon|IM)$  on  $M_w$  and  $\ln(R_{clst})$  (refer to Luco and Cornell (2007) for more details). The  $p$ -value obtained from the linear regression indicates the degree of sufficiency, where a small  $p$ -value (e.g., less than 0.05) suggests that the *IM* is insufficient, and a larger  $p$ -value indicates stronger evidence of a sufficient *IM*.

Another feature that an appropriate *IM* should also possess is the hazard computability, which refers to the effort required to compute the seismic hazard or determine the hazard curve in terms of the *IM* (Giovenale *et al.* 2004). Currently, different peak ground parameters and spectral quantities, e.g., PGA and  $S_{a-1}$ , spectral acceleration at 1 s, have been easily used to estimate the seismic hazard of the most seismically active regions worldwide by seismologists and geotechnical earthquake engineers, while some other *IMs* will likely be very structure specific, which means that more information and efforts are required to determine the seismic hazard of a site. Hence, the feasibility of computing the seismic hazard in terms of the proposed *IM* should be considered.

## 7. Comparison of different *IMs*

Using the linear regression model introduced in Section 6, the measure  $D$ , which is chosen as  $DI$  in the present study, obtained from incremental dynamic analyses of the aforementioned single-layer reticulated dome is regressed on the 11 different *IMs* presented in Section 3.2 together with the newly proposed  $S_{a, dom}$ . To conduct a comprehensive examination of the appropriateness and superiority in terms of correlation, efficiency, and sufficiency of  $S_{a, dom}$  relative to the other 11 *IMs*, three different cases of ground motion inputs are considered in this study, i.e., unidirectional horizontal, unidirectional vertical, and tri-directional ground motion excitations. The detailed comparison results are listed as follows.

### 7.1 Unidirectional horizontal seismic excitation

For a single-layer reticulated dome subjected to unidirectional horizontal ground acceleration, its total seismic response is nearly determined by the combination of a number of dominant vibration modes which always includes several higher modes, rather than an individual vibration mode (e.g., the fundamental mode). As a result, it is expected that *IMs* incorporating more ground motion frequency content associated with the dominant vibration modes would be more closely related to the total seismic response of a reticulated dome.

Fig. 5 shows the results of natural logarithmic regression of  $DI$  on the 12 different *IMs* when the reticulated dome is subjected to unidirectional horizontal seismic excitation. Here the acceleration with a larger PGA value between the two horizontal components is chosen as the seismic input in the X-direction and all the *IMs* are calculated on the basis of the corresponding component. As can be clearly seen,  $S_{a, dom}$  involving spectral accelerations at multiple dominant modes is most strongly correlated with the  $DI$  of the single-layer reticulated dome, having the largest  $\rho$  of 0.930. Among the other 11 *IMs*, the acceleration spectrum intensity, ASI, with the second largest  $\rho$  of 0.891, performs relatively better than the other spectral acceleration-based quantities, i.e.,  $S_a(T_1)$ ,  $S_a(f_p)$ ,  $S_{a, avg}$  and  $I_{Np}$ , despite the latter two have a wide range of periods incorporated, which is due in part to the number of dominant vibration modes involved in the

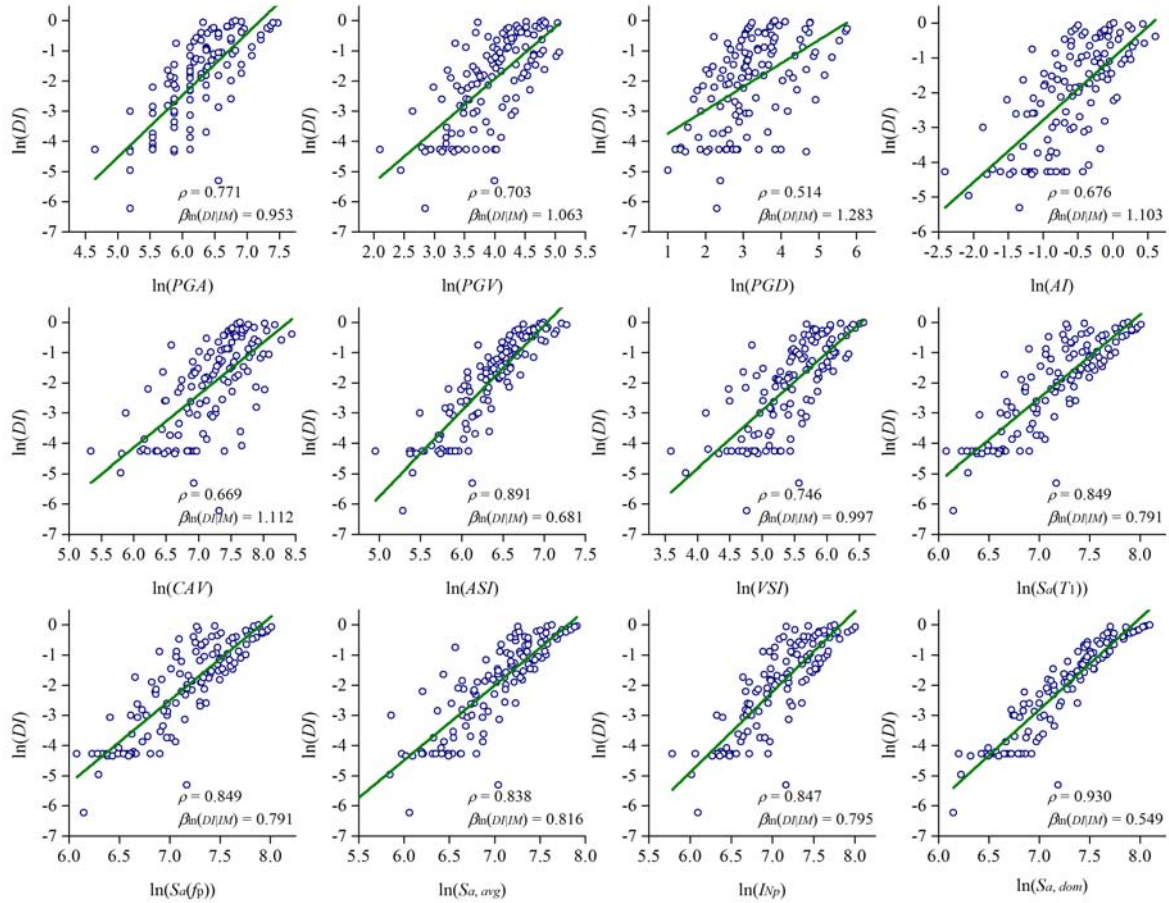


Fig. 5 Results of the natural logarithmic regression of the *DI* on the 12 different *IMs* for the single-layer reticulated dome under unidirectional horizontal seismic excitation

calculation of these five spectrally-based *IMs*. Obviously, *ASI* is capable of incorporating all the dominant modes, for it was the integration of spectral acceleration over the periods from 0 to 0.5 s; both of  $S_a(T_1)$  and  $S_a(f_p)$  can involve the fundamental mode, which is the most dominant vibration mode, while  $I_{Np}$  can also have the fundamental mode involved, for it was calculated over 10 logarithmic spaced periods from  $T_1$  to  $2.0T_1$ , yet none of the 10 log-spaced periods from  $0.25T_1$  to  $2.5T_1$  involved in the calculation of  $S_{a, avg}$  matches any of the dominant modes. Among the remaining *IMs*, the commonly used *PGA* shows stronger evidence of good correlation with the *DI*; however, it is not desirable in comparison with the preceding higher performing *IMs* in terms of correlation.

As alluded to above in Section 6,  $\beta_{\ln(DI/IM)}$  serves as a viable measure of the relative efficiency of an *IM*. Here, as evidenced by Fig. 5, the smallest scatter about the regression fit (quantified by  $\beta_{\ln(DI/IM)}=0.549$ ) indicates that the newly proposed  $S_{a, dom}$  is the most efficient *IM* among the 12 potential *IMs*, followed by *ASI*,  $S_a(T_1)$ ,  $S_a(f_p)$ ,  $I_{Np}$  and  $S_{a, avg}$ , for which  $\beta_{\ln(DI/IM)}$  are 0.681, 0.791, 0.791, 0.795 and 0.816, respectively. Conversely, the remaining *IMs* exhibit weak correlations with the *DI*, and accordingly show poor evidence of an efficient *IM*. For example,  $\beta_{\ln(DI/IM)}$  for the *DI* are

0.953, 1.283, and 0.997 for PGA, PGD, and velocity spectrum intensity, VSI, respectively.

7.2 Unidirectional vertical seismic excitation

Fig. 6 presents the regression analysis results of natural logarithms of the  $DI$  on the corresponding values of the 12 different  $IMs$  for the single-layer reticulated dome under unidirectional vertical seismic excitation. Here the vertical component of each ground motion is chosen as the seismic input in the Z-direction and accordingly all the  $IMs$  are calculated based on this component. The regression results show that the degree of correlation between the newly proposed  $S_{a, dom}$  and the  $DI$  is much larger than that of the other 11  $IMs$ . Specifically speaking,  $S_{a, dom}$  has the largest  $\rho$  of 0.808, and the corresponding values for  $S_a(f_p)$ , ASI,  $S_{a, avg}$ ,  $I_{Np}$  and  $S_a(T_1)$  are 0.743, 0.680, 0.671, 0.501 and 0.426, respectively. Among all but the newly proposed  $IM$ ,  $S_a(f_p)$  is obviously most strongly correlated with the nonlinear structural response (here the  $DI$ ), which is consistent with the previous conclusion drawn by Fan *et al.* (2012) that  $S_a(f_p)$  is more closely related to the linear elastic seismic response (the maximum elastic displacement over all nodes) than  $S_a(T_1)$ , ASI, PGA, and so forth in the case of unidirectional vertical seismic excitation.

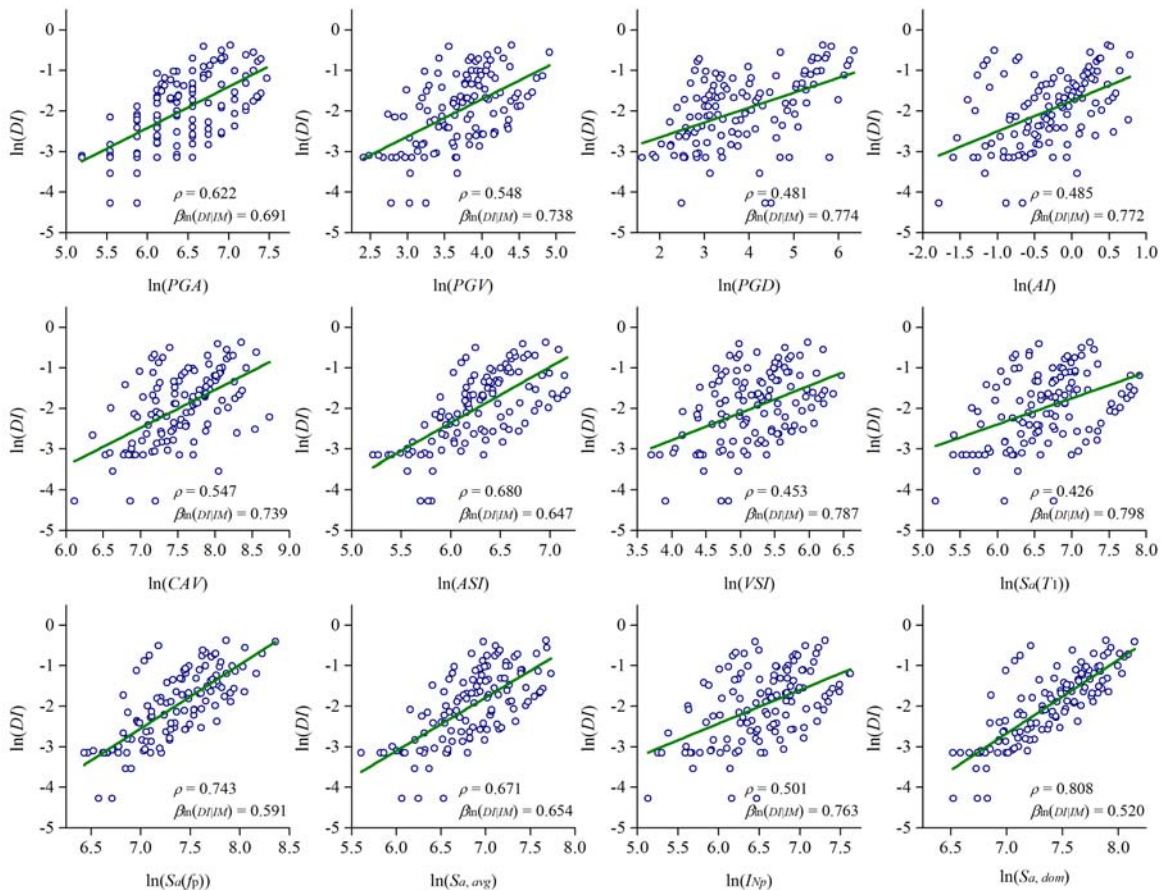


Fig. 6 Results of natural logarithmic regression of the  $DI$  on the 12 different  $IMs$  for the single-layer reticulated dome under unidirectional vertical seismic excitation

Nonetheless, the newly proposed  $S_{a, dom}$  performs much better than  $S_a(f_p)$  due to the fact that the latter does not take account of the contribution of other higher modes except the mode associated with the peak response frequency. Interestingly, in this case, ASI,  $S_{a, avg}$ ,  $I_{Np}$ , which have relatively strong correlation in the case of unidirectional horizontal seismic excitation, are no longer strongly correlated with the seismic response. The most important reason may be that the manner in which these *IMs* take into account the frequency content of a ground motion and the higher mode effects underestimates the contributions of the limited number of higher modes that are within a relatively narrow period range, or does not involve the necessary dominant modes.

Similarly, the newly proposed  $S_{a, dom}$  appears to be the most efficient *IM* with a relatively low conditional dispersion ( $\beta_{\ln(DI|IM)}=0.520$ ), followed by  $S_a(f_p)$  with a slightly larger  $\beta_{\ln(DI|IM)}$  of 0.591, which implies again that consideration of the contributions of multiple dominant vibration modes can indeed contribute to a more accurate prediction of the seismic response of single-layer reticulated domes. It should also be noted that none of the other 10 *IMs* tends to lead to less seismic response variability. Therefore, in terms of correlation and efficiency, it can also be concluded in this case that  $S_{a, dom}$  is the most appropriate *IM* for use in the prediction of the structural response of single-layer reticulated domes due to unidirectional vertical seismic excitation.

### 7.3 Tri-directional seismic excitation

The seismic performance of a single-layer reticulated dome is always evaluated by performing full three-dimensional nonlinear dynamic analysis. Hence, of greatest importance in the present study is to examine thoroughly the appropriateness and superiority of  $S_{a, dom}$  in the case of quantifying the strength of a tri-directional ground motion as a whole with respect to the other 11 *IMs* in terms of correlation, efficiency, and sufficiency. In this case, the newly proposed  $S_{a, dom}$  is calculated as illustrated in Section 4.2 while the other 11 *IMs* are calculated as the SRSS combination of the corresponding values of the three components of the ground motion. The regressions of the *DI* on the 12 different *IMs* are illustrated in Fig. 7. As evidenced by the estimated values of  $\rho$ , the newly proposed  $S_{a, dom}$  is rather strongly correlated with the *DI*, with a large  $\rho$  value of 0.938, whereas ASI and  $S_{a, avg}$  exhibit the appropriately equally strong degree of correlation ( $\rho=0.901$  and 0.898, respectively), followed by  $S_a(T_1)$ ,  $I_{Np}$ , PGA, VSI, and  $S_a(f_p)$ . One may also find that all the other *IMs* are much less likely to be strongly correlated with the nonlinear seismic response of a single-layer reticulated dome.

The rather small scatter observed about the regression fit ( $\beta_{\ln(DI|IM)}=0.521$ ) indicates that the newly proposed  $S_{a, dom}$  is fairly efficient. Likewise, ASI and  $S_{a, avg}$  also exhibit a higher efficiency relative to the other 10 *IMs*. Moreover, it is interesting to note that *IMs* exhibiting strong correlation generally exhibit high efficiency as well, while those with weak correlation tend to exhibit poor efficiency.

The sufficiency values of the aforementioned six *IMs* with relatively good correlation and efficiency in the case of tri-directional seismic excitation (i.e.,  $S_{a, dom}$ ,  $S_{a, avg}$ ,  $I_{Np}$ , PGA, ASI, and  $S_a(T_1)$ ) are compared via examination of the conditional dependence from  $M_w$  and  $R_{clst}$ . As described in Section 6, the  $p$ -value is a good indicator for the sufficiency of an *IM*, and we recall that a low  $p$ -value (here, less than 0.05) indicates that the *IM* is insufficient. For brevity, Fig. 8 presents the linear regressions of the observed residuals,  $\ln(\varepsilon|IM)$ , (from the preceding natural logarithmic regression of *DI* on  $S_{a, dom}$ ) on  $M_w$  and  $\ln(R_{clst})$ . We note from Fig. 8 that the  $p$ -values are both greater than the cutoff value of 0.05, with relatively large values of 0.721 and 0.811,

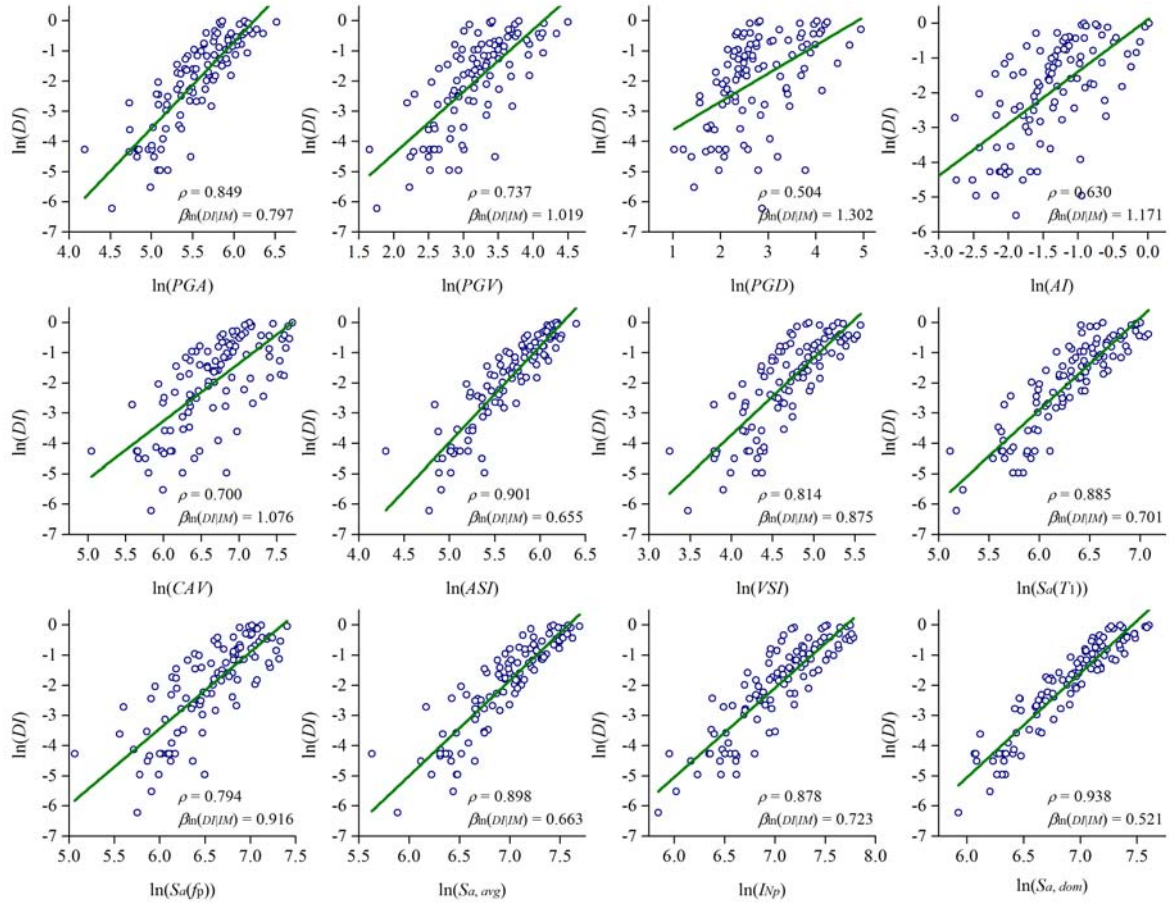


Fig. 7 Results of natural logarithmic regression of the  $DI$  on the 12 different  $IM$ s for the single-layer reticulated dome under tri-directional seismic excitation

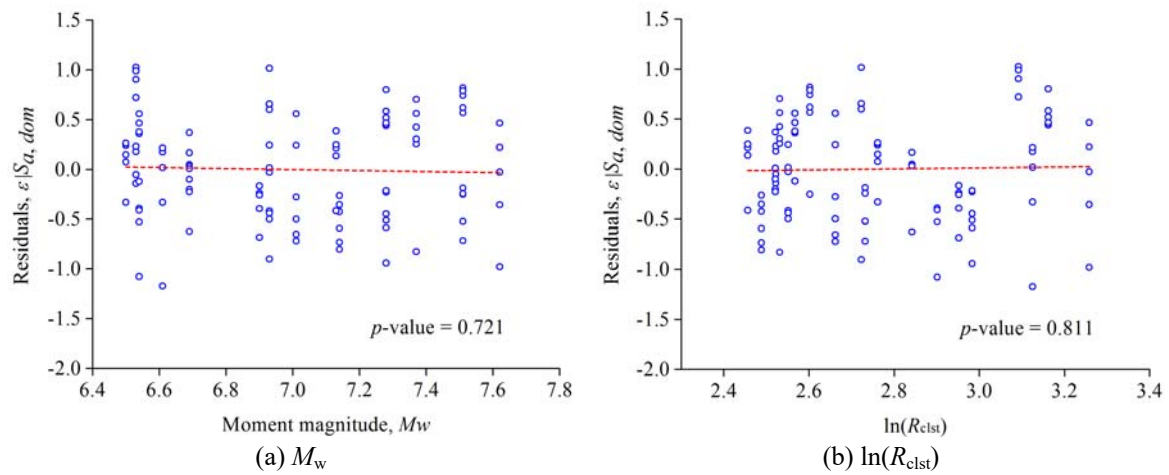


Fig. 8 Linear regression results of residuals on  $M_w$  and  $R_{clst}$  for  $S_{a,dom}$

Table 5 Summaries of the correlation, efficiency, and sufficiency of the 6 selected IMs in the case of tri-directional seismic excitation

Intensity measure	$\rho$	$\beta_{\ln(DI/IM)}$	$p$ -value	
			$M_w$	$\ln(R_{clst})$
<i>PGA</i>	0.849	0.797	0.167	0.253
<i>ASI</i>	0.901	0.655	0.418	0.683
$S_a(T_1)$	0.885	0.663	0.412	0.034
$S_{a,avg}$	0.898	0.663	0.533	0.686
$I_{Np}$	0.878	0.723	0.499	0.759
$S_{a, dom}$	0.938	0.521	0.721	0.811

respectively, indicating that  $S_{a, dom}$  is conditionally independent from  $M_w$  and  $R_{clst}$ , and, in short, sufficient. Furthermore, Table 5 summarizes the  $p$ -values of the other five IMs. It is clear that, except that  $S_a(T_1)$  is observed to demonstrate conditional dependence on  $R_{clst}$ , the other five IMs prove to be sufficient regardless of  $M_w$  and  $R_{clst}$ .

The above comparison results indicate that the newly proposed  $S_{a, dom}$  is rather strongly correlated with the  $DI$ , and is also the most efficient and sufficient IM among the 12 different IMs considered in this study. Hence, it is a more appropriate IM for use in predicting seismic response.

### 8. Hazard computability of $S_{a, dom}$

As a matter of fact, hazard computability is another crucial criterion for evaluating the applicability of a newly-proposed IM, along with the above discussed criteria, i.e., correlation, efficiency and sufficiency. It refers to the possibility of assessing the probabilistic seismic hazard or determine the hazard curve. In order to facilitate the application of  $S_{a, dom}$ , its hazard computability is discussed in this section. Here, applying the natural logarithm to Eq. (1), it results in

$$\ln(S_{a, dom}) = \sum_{i=1}^N r_i \ln[S_a(T_i^d, \xi)] \tag{18}$$

Hence, the mean and variance of  $\ln(S_{a, dom})$  can be expressed as

$$E[\ln(S_{a, dom})] = \sum_{i=1}^N r_i E\{\ln[S_a(T_i^d, \xi)]\} \tag{19}$$

$$\begin{aligned} Var[\ln(S_{a, dom})] &= \sum_{i=1}^N r_i^2 Var\{\ln[S_a(T_i^d, \xi)]\} \\ &+ 2 \sum_{i=1}^N \sum_{j \neq i}^N r_i r_j \rho_{\ln[S_a(T_i^d, \xi)], \ln[S_a(T_j^d, \xi)]} \sigma_{\ln[S_a(T_i^d, \xi)]} \sigma_{\ln[S_a(T_j^d, \xi)]} \end{aligned} \tag{20}$$

Since the  $\ln[S_a(T_i^d, \xi)]$  values are commonly assumed to follow jointly Gaussian distribution (Bazzurro and Cornell 2002, Stewart *et al.* 2002), and hence the sum in Eq. (18) is obviously

Gaussian. In Eq. (20),  $\rho_{\ln[S_a(T_i^d, \xi)], \ln[S_a(T_j^d, \xi)]}$  can be evaluated for example by the relationship expressed as Eq. (21) (Inoue and Cornell 1990).

$$\rho_{\ln[S_a(T_i^d, \xi)], \ln[S_a(T_j^d, \xi)]} = 1 - 0.33 |\ln(1/T_i^d) - \ln(1/T_j^d)| \quad (21)$$

Finally, because the  $\ln[S_a(T_i^d, \xi)]$  values are jointly Gaussian, Eqs. (19)-(20) can be obtained from the actual attenuation models, and these two parameters are enough to describe the probability distribution of  $\ln(S_{a, dom})$ , which can be used to perform the probabilistic seismic hazard analysis.

## 9. Conclusions

This study has proposed a scalar ground motion  $IM$  (i.e.,  $S_{a, dom}$ ) based on the dominant vibration modes of single-layer reticulated domes. In particular,  $S_{a, dom}$  was calculated as the weighted geometric mean of the spectral accelerations at periods associated with the dominant vibration modes, where the modal strain energy ratio of each mode was the corresponding weight. The appropriateness of  $S_{a, dom}$  was investigated in terms of correlation with the nonlinear seismic response, efficiency, sufficiency and hazard computability, for different cases of seismic excitation, i.e., unidirectional horizontal, vertical, and tri-directional ground motion input.

In the case of unidirectional horizontal seismic excitation, the dominant vibration mode-based  $S_{a, dom}$  was determined to be much more strongly correlated with the nonlinear seismic response and also more efficient than the other spectrally based  $IMs$  or peak ground parameters, e.g.,  $S_{a, avg}$ ,  $I_{Np}$ , PGA, which is more likely to be attributed to the fact that the total seismic response in this case is actually determined by a number of dominant modes within a wide frequency range, and the inclusion of spectral accelerations at multiple dominant modes more precisely captures the frequency content of a ground motion at the corresponding modes, including the higher ones. In the unidirectional vertical excitation case,  $S_{a, dom}$  was also deemed superior on the basis of stronger correlation and higher efficiency. In the case of tri-directional seismic excitation, the newly proposed  $S_{a, dom}$  was further demonstrated to be an optimal  $IM$  based on all the metrics considered in this paper. It was found that the degrees of both correlation and efficiency of each  $IM$  in this case were very similar to those in the unidirectional horizontal case because the structural response of a single-layer reticulated dome under tri-directional ground motion excitation is typically determined by the largest component of each ground motion, i.e., the horizontal component used in the first case. Besides, the sufficiency comparison illustrated that  $S_{a, dom}$  has as good sufficiency as other spectrally based  $IMs$ , e.g.,  $S_{a, avg}$  and  $I_{Np}$ .

Finally, the hazard computability of  $S_{a, dom}$  was briefly discussed and illustrated, and it was demonstrated that the probabilistic hazard analysis for  $S_{a, dom}$  can be performed using existing assumptions and techniques. Therefore, it can be concluded that this dominant vibration mode-based  $S_{a, dom}$  is the most appropriate  $IM$  of those considered for use in the probabilistic seismic performance assessment of single-layer reticulated domes or other similar long-span spatial lattice structures.

## Acknowledgments

This research was financially supported by the National Natural Science Foundation of China (Grant Nos: 51278152, 51525802 and 91315301.) and the China Scholarship Council as well as the National Key Technology R&D Program (No. 2015BAK17B03). The very constructive comments by the reviewers to this paper are also greatly appreciated.

## References

- ATC (2009), *FEMA P695: Quantification of building seismic performance factors*, ATC-63, Applied Technology Council, Redwood City, CA, USA.
- Bazzurro, P. and Cornell, C.A. (2002), "Vector-valued probabilistic seismic hazard analysis", *Proceedings of the 7th U.S. National Conference on Earthquake Engineering*, Massachusetts, USA.
- Bianchini, M., Diotallevi, P.P. and Baker, J.W. (2009), "Prediction of inelastic structural response using an average of spectral accelerations", *Proceedings of the 10th International Conference on Structural Safety and Reliability (ICOSSAR09)*, Osaka, Japan.
- Bojórquez, E. and Iervolino, I. (2011), "Spectral shape proxies and nonlinear structural response", *Soil. Dyn. Earthq. Eng.*, **31**(7), 996-1008.
- BSSC (1997), *NEHRP guidelines for the seismic rehabilitation of buildings*, FEMA-273, developed by ATC for FEMA, Washington, D.C., USA.
- Chopra, A.K. (2001), *Dynamics of Structures: Theory and Applications to Earthquake Engineering*. Prentice Hall: Englewood Cliffs, New Jersey, USA.
- Cordova, P.P., Deierlein, G.G., Mehanny, S.S.F. and Cornell, C.A. (2000), "Development of a two-parameter seismic intensity measure and probabilistic assessment procedure", *Proceedings of the 2nd U.S.-Japan Workshop on Performance-Based Seismic Design Methodology for Reinforced Concrete Building Structures*, California, USA.
- Cornell, C.A., Jalayer, F., Hamburger, R.O. and Foutch, D.A. (2002), "Probabilistic Basis for 2000 SAC Federal Emergency Management Agency steel moment frame guidelines", *J. Struct. Eng.*, **128**(4), 526-533.
- Ellingwood, R.R., Celik, O.C. and Kinali, K. (2007), "Fragility assessment of building structural systems in Mid-America", *Earthq. Eng. Struct. Dyn.*, **36**(13), 1935-1952.
- Fan, F., Li, Y.G. and Hong, H.P. (2012), "Study on one-dimensional earthquake intensities for Kiewitt-8 single-layer reticulated domes", *J. Build. Struct.*, **33**(12), 72-78.
- GB50011-2010 (2010), *Code for seismic design of buildings*, China Architecture and Building Press, Beijing.
- Giovenale, P., Cornell, C.A. and Esteva, L. (2004), "Comparing the adequacy of alternative ground motion intensity measures for the estimation of structural responses", *Earthq. Eng. Struct. Dyn.*, **33**(8), 951-979.
- Inoue, T. and Cornell, C.A. (1990), "Seismic hazard analysis of multi-degree-of-freedom structures", Reliability of marine structures, RMS-8. Stanford University, CA, USA.
- Jayaram, N., Bazzurro, P., Mollaioli, F., Sortis, A.D. and Bruno, S. (2010), "Prediction of structural response in reinforced concrete frames subjected to earthquake ground motions", *Proceedings of the 9th U.S. National and 10th Canadian Conference on Earthquake Engineering*, Toronto, Canada.
- JGJ7-2010 (2010), *Technical Specification for Space Frame Structures*, China Architecture and Building Press, Beijing, China.
- Kato, S., Nakazawa, S. and Saito, K. (2007), "Estimation of static seismic loads for latticed domes supported by substructure frames with braces deteriorated due to buckling", *J. Int. Assoc. Shell Spatial Struct.*, **48**(2), 71-86.
- Kostinakis, K.G. and Athanatopoulou, A.M. (2015), "Evaluation of scalar structure-specific ground motion intensity measures for seismic response prediction of earthquake resistant 3D buildings", *Earthq. Struct.*, **9**(5), 1091-1114.

- Luco, N. and Cornell, A.C. (2007), "Structure-specific scalar intensity measures for near-source and ordinary earthquake ground motions", *Earthq. Spectra.*, **23**(2), 357-392.
- Luco, N., Manuel, L., Baldava, S. and Bazzurro, P. (2005), "Correlation of damage of steel moment-resisting frames to a vector-valued set of ground motion parameter", *Proceedings of the 9th International Conference on Structural Safety and Reliability (ICOSSAR05)*, Rome, Italy.
- Nie, G.B., Fan, F. and Zhi, X.D. (2012), "A constitutive model for circular steel pipe by spatial hysteretic test", *Adv. Struct. Eng.*, **15**(8), 1279-1290.
- Nielson, B.G. and DesRoches, R. (2007), "Analytical seismic fragility curves for typical bridges in the central and southeastern United States", *Earthq. Spectra.*, **23**(3), 615-633.
- Padgett, J.E., Nielson, B.G. and DesRoches, R. (2008), "Selection of optimal intensity measures in probabilistic seismic demand models of highway bridge portfolios", *Earthq. Eng. Struct. Dyn.*, **37**(5), 711-725.
- Shome, N. (1999), "Probabilistic seismic demand analysis of non-linear structures", Ph.D. Dissertation, Stanford University, CA, USA.
- Shome, N., Cornell, C.A., Bazzurro, P. and Carballo, J.E. (1998), "Earthquakes, records, and nonlinear responses", *Earthq. Spectra.*, **14**(3), 469-500.
- Stewart, J.P., Chiou, S.J., Bray, J.D., Somerville, P.G. and Abrahamson, N.A. (2002), "Ground motion evaluation procedures for performance-based design", *Soil. Dyn. Earthq. Eng.*, **22**(9), 765-772.
- Vamvatsikos, D. and Cornell, C.A. (2002), "Incremental dynamic analysis", *Earthq. Eng. Struct. Dyn.*, **31**(3), 491-514.
- Yang, D.B., Zhang, Y.G. and Wu, J.Z. (2010), "Computation of Rayleigh damping coefficients in seismic time-history analysis of spatial structures", *J. Int. Assoc. Shell Spatial Struct.*, **51**(2), 125-135.
- Zhi, X.D., Nie, G.B., Fan, F. and Shen, S.Z. (2012), "Vulnerability and risk assessment of single-layer reticulated domes subjected to earthquakes", *J. Struct. Eng.*, **138**(12), 125-135.